

Magnetic resonance elastography of the brain

Scott A. Kruse, Gregory H. Rose, Kevin J. Glaser, Armando Manduca, Joel P. Felmlee, Clifford R. Jack Jr., and Richard L. Ehman*

Mayo Clinic, Department of Radiology, 200 First Street Southwest, Rochester, MN 55905, USA

Received 30 March 2007; revised 10 July 2007; accepted 10 August 2007

Available online 29 August 2007

The purpose of this study was to obtain normative data using magnetic resonance elastography (MRE) (a) to obtain estimates of the shear modulus of human cerebral tissue *in vivo* and (b) to assess a possible age dependence of the shear modulus of cerebral tissue in healthy adult volunteers. MR elastography studies were performed on tissue-simulating gelatin phantoms and 25 healthy adult volunteers. The data were analyzed using spatiotemporal filters and a local frequency estimating algorithm. Statistical analysis was performed using a paired *t*-test. The mean shear stiffness of cerebral white matter was 13.6 kPa (95% CI 12.3 to 14.8 kPa); while that of gray matter was lower at 5.22 kPa (95% CI 4.76 to 5.66 kPa). The difference was statistically significant ($p < 0.0001$).

© 2007 Published by Elsevier Inc.

Keywords: Magnetic resonance elastography; Shear stiffness; Elasticity; Mechanical properties; Tissue characterization; Brain

Introduction

While many diagnostic imaging techniques have emerged over the last few decades, palpation remains a useful technique to localize lesions on the basis of their differential stiffness compared to surrounding tissues. Abnormal tissues commonly display a shear modulus up to 100 times that of normal tissue (Duck, 1990; Sarvazyan et al., 1994). These observations have prompted the development of techniques to quantitatively image the elastic modulus of various normal and abnormal tissues (Bishop et al., 1998; Chenevert et al., 1998; Fowlkes et al., 1995; Lewa and de Certaines, 1995; Muthupillai et al., 1995; Ophir et al., 1991; Parker et al., 1990; Parker and Lerner, 1992; Plewes et al., 1995; Van Houten et al., 1999). Conventional imaging modalities such as radiography, computed tomography (CT), ultrasound (US) and magnetic resonance imaging (MRI) are not capable of directly assessing the mechanical properties of tissue.

Magnetic resonance elastography (MRE) is a noninvasive technique that allows for the determination of the shear modulus (elastic modulus, shear stiffness) of tissues *in vivo* (Ehman et al., 1995; Muthupillai and Ehman, 1996; Muthupillai et al., 1995, 1996). This technique requires the application of shear waves to tissue (with frequencies in the acoustic range), a phase-sensitive MR imaging sequence to detect the propagating waves and an algorithm to generate an elastic modulus map of the tissue of interest (Manduca et al., 2001).

While there is no clinical precedent for “brain palpation”, measurements of brain elastic properties may have useful applications for characterizing brain disease. For example, some diffuse diseases of the brain are poorly evaluated by conventional imaging techniques. Processes such as Alzheimer's disease slowly replace normal brain tissue with senile plaques and neurofibrillary tangles. It is possible that such diffuse infiltration may affect the mechanical properties of cerebral tissue. It has also been hypothesized that certain diseases, such as normal pressure hydrocephalus, may be caused by changes in the mechanical properties of the brain (Bradley et al., 1991). It is also possible that quantitative imaging of the mechanical properties of tissue may be useful in the characterization of focal brain lesions. Valid quantitative measurements of the elastic modulus of cerebral tissue are also of interest in biomechanical studies of brain trauma and in the development of neurosurgery simulation techniques (Kleiven and Hardy, 2002; Miga and Paulsen, 2000; Miller, 1999; Roberts et al., 1999; Zhang et al., 2001). To date, the available estimates of the shear modulus of brain tissue in the literature are inconsistent (Fig. 1).

The purpose of this study was to develop techniques to evaluate the feasibility of magnetic resonance elastography of the brain *in vivo*. The specific goals were (a) to obtain estimates of the shear modulus of human cerebral tissue and (b) to assess the age dependence of the shear modulus in healthy volunteers.

Materials and methods

Magnetic resonance elastography theory

The MR elastography technique has been described in numerous publications to date (Manduca et al., 2001; Muthupillai and Ehman,

* Corresponding author. Fax: +1 507 284 9778.

E-mail address: ehman.richard@mayo.edu (R.L. Ehman).

Available online on ScienceDirect (www.sciencedirect.com).

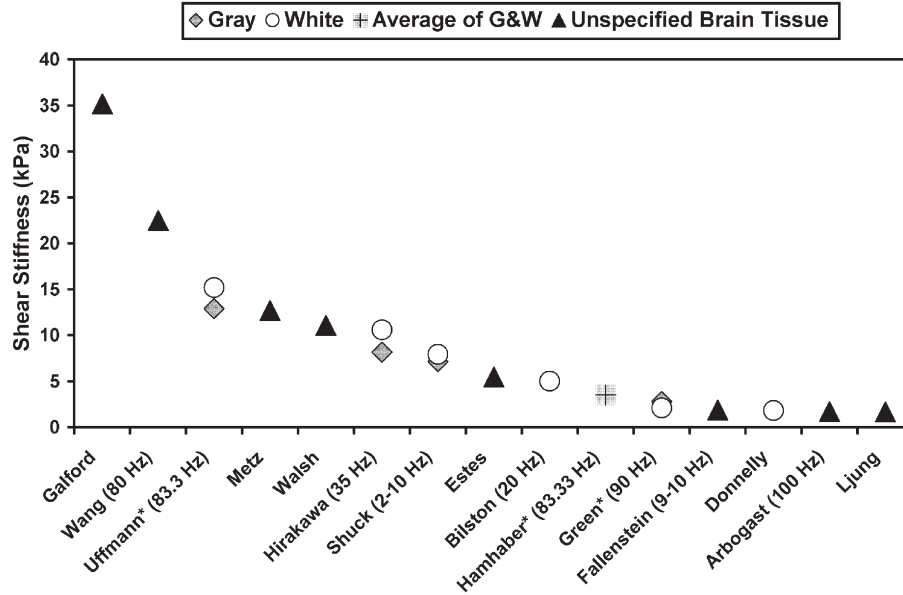


Fig. 1. Shear stiffness measurements in the literature of mammalian brain tissue (Arbogast and Margulies, 1998; Bilston et al., 1997; Donnelly and Medige, 1997; Estes and McElhane, 1970; Fallenstein et al., 1969; Galford and McElhane, 1970; Green et al., 2006; Hamhaber et al., 2007; Hirakawa et al., 1981; Ljung, 1975; Metz et al., 1970; Shuck and Advani, 1972; Uffmann et al., 2004; Walsh and Schettini, 1976; Wang and Wineman, 1972). The studies were performed *in vitro*, *ex vivo* and *in vivo* (denoted by *) using a variety of experimental techniques (shear/strain, load cell, pressure transducer, vibrating probe and MR elastography). The frequency of dynamic testing is indicated. The shear wave speed was calculated from the real and imaginary parts of the complex modulus (Auld, 1990; Oliphant et al., 2001). The result was then entered into Eq. (2) to calculate shear stiffness.

1996; Muthupillai et al., 1995, 1996). Therefore, the image acquisition and processing will only be summarized here. MR elastography has three essential components. They are (a) an acoustic actuator which is coupled to the tissue of interest to induce shear wave motion, (b) a pulse sequence using phase-locked cyclic motion-sensitizing gradients to encode the motion as phase in the MR images and (c) an inversion algorithm that uses the measured displacements to calculate the shear modulus distribution in the tissue.

The phase shift induced in the received NMR signal by cyclic motion at the location r caused by a mechanical wave propagating within a medium at a given frequency, in the presence of a cyclic motion-encoding gradient at the same frequency, is given by the following expression:

$$\varphi(\vec{r}, \theta) = \frac{2\gamma NT(\vec{G}_0 \cdot \vec{\xi}_0)}{\pi} \cos(\vec{k} \cdot \vec{r} + \theta) \quad (1)$$

The accumulated phase shift φ is proportional to the dot product of the gradient vector \vec{G}_0 and the displacement vector $\vec{\xi}_0$, the number of gradient cycles (N) and the period of the gradient waveform (T). The quantity θ is the phase relationship between the motion-encoding gradient and the motion at r due to the externally applied mechanical excitation, \vec{k} is the shear wave vector, \vec{r} is the position vector and γ is the gyromagnetic ratio. The dot product relationship indicates that displacements occurring along any direction can be measured by changing the direction of the applied gradients. As with other phase-contrast-based techniques, two measurements are acquired with alternate polarities of the motion-encoding gradients. The phase images from each acquisition are then subtracted to yield a phase difference image that reflects the phase shift caused by the propagating mechanical wave. By accumulating phase during several wave cycles, the technique can

depict cyclic motions with amplitudes less than 100 nanometers (Muthupillai et al., 1995).

Acoustic actuator

The method for imaging propagating mechanical waves in the brain has been previously described (Fig. 2) (Felmlee et al., 1997; Moore et al., 2003; Rose et al., 1998; Smith et al., 1997; Xu et al., 2007). In one actuator design, the subject would lie supine with his/her head on a cradle attached to an electromechanical actuator with a restraining band across the forehead to ensure coupling of the vibration (Kruse et al., 1999). The electromechanical actuator vibrated the head in the antero-posterior direction. The actuator coils were inside the imaging coil and in some cases caused artifacts in the posterior of the head. In later cases, a thermoplastic “bite block” was fit to each volunteer (Kruse and Ehman, 2003). The bite block was attached to an electromechanical actuator that vibrated the head in the right-left direction. The bite block actuator was more comfortable for the volunteers. In both cases, the applied global head vibration generated low-amplitude shear waves that originated at meningeal surfaces. This is thought to be due to an inertial effect, with coupling between the skull and brain (across the arachnoid space) by the trabeculae of the pia mater.

MRE acquisition

All MR data acquisitions were performed on a 1.5-T GE Signa System (General Electric, Milwaukee, WI) using a modified gradient-echo (GRE) pulse sequence. In addition to the standard imaging gradients, the MRI sequence incorporated oscillating motion-sensitizing gradients that were synchronized with the acoustic shear

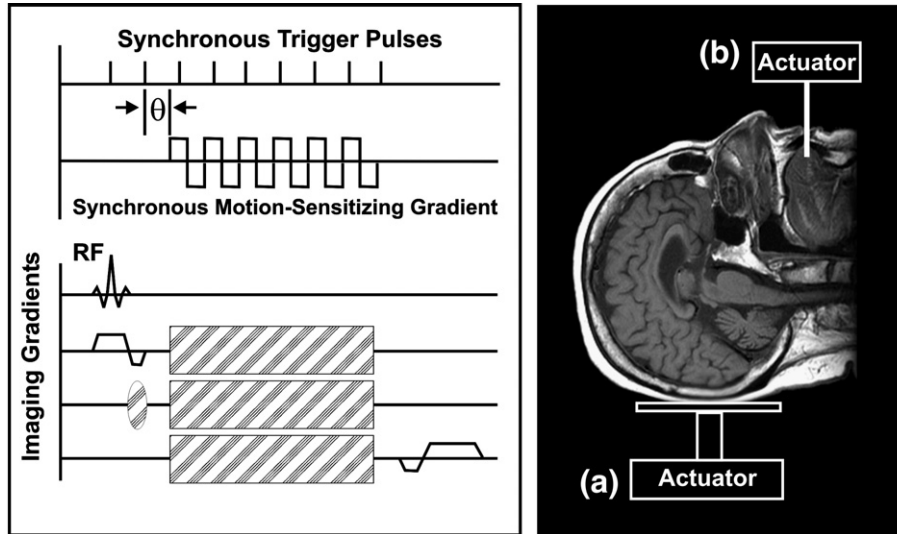


Fig. 2. Schematic diagram of the magnetic resonance elastography system. Conventional MR imaging gradients and RF pulses that encode spatial positions are shown at the bottom left. The electromechanical actuator (a) applies vertical displacement to the object to be imaged via a cradle or (b) horizontal displacement via a bite block (right). The cyclic motion-sensitizing gradients and the actuator are synchronized using trigger pulses provided by the imager. The phase offset (θ) between the two can be varied to image the waves at various stages of propagation. As shown by the shaded regions, the motion-sensitizing gradients can be superimposed along any desired axis to detect that component of the cyclic motion vector. All data was collected and analyzed using 100 Hz motion.

waves. The MRE scanning parameters included the following: a pulse repetition time (TR) of 100–200 ms, an echo time (TE) of 40–50 ms, a flip angle of 40° , an acquisition matrix of 256×64 , a slice thickness of 5 mm, a field of view (FOV) of 20–24 cm and one pair of interleaved toggling motion-encoding gradients acquired for each phase encoding view, resulting in an acquisition time of 13–26 sec. In each volunteer study, this sequence was repeated 8 times with incremental values of θ (the phase lag between the motion-encoding waveform and the applied mechanical waves) from 0 to 2π in order to provide wave images at multiple points over one cycle of the motion.

Summary of inversion processing

The mechanical property called the shear modulus (μ) describes the proportionality relationship between transverse stress and strain in a simple isotropic linear elastic material. The speed of propagation (v) of planar shear waves in simple isotropic Hookean materials is related to the density (ρ) and the shear modulus by the following relationship (Graff, 1991):

$$\mu = v^2 \rho \quad (2)$$

The propagation speed of shear waves can be calculated from the wavelength (λ) and the frequency of the externally applied mechanical excitation (f) as follows:

$$v = f\lambda \quad (3)$$

Hence, if the local wavelength is measured in an image of propagating shear waves, the shear modulus can be estimated using Eqs. (2) and (3). A further simplification is that a good approximation for the density of most soft tissues is that of water ($\rho = 1 \text{ g cm}^{-3}$) (Burlew et al., 1980). Technically, the shear modulus of a material refers to a static stress and in attenuating materials the

quantity calculated above can vary with frequency (Auld, 1990). We therefore use the term shear stiffness to indicate the “effective” shear modulus of an object at a specific frequency.

In complex wave fields, with reflections, interference, etc., the wave field (under certain assumptions) may still be regarded as the superposition of waves with different amplitudes propagating in different directions, but sharing the same underlying wavelength. The local wavelength at each point in the image is calculated with a local spatial frequency estimation algorithm (denoted LFE) that estimates this underlying wavelength (Knutsson et al., 1994). More details of the algorithm and the underlying assumptions are given in Manduca et al. (1996, 2001).

Each set of wave images was processed using a set of spatio-temporal filters to decompose the complex wave fields into components propagating in different directions (Manduca et al., 2003). The LFE algorithm was applied to each directionally filtered data set to extract the local wavelength and compute quantitative shear stiffness maps (Manduca et al., 2001). The maps based on individual propagation directions were recombined using an amplitude squared weighting based on the amplitude of the filtered wave motion. T2-weighted images were used to select regions of interest (ROI) in the gray matter and white matter. The phase difference SNR (the ratio between the amplitude of the displacement phase data to the phase noise) was verified to be greater than 5:1 in each region of interest. The shear modulus maps were then analyzed by calculating the mean and standard deviation of four regions of interest, consisting of 100–200 pixels. The regions were chosen by one of the authors for all of the analysis. The exact locations for each volunteer were chosen following inspection of the T2-weighted images for large homogeneous regions of gray white and white matter. This was done to minimize partial volume and boundary effects in the ROIs. Because of intrinsic assumptions, such as local tissue homogeneity, tissue boundaries are not expected to be resolved correctly. Therefore, the regions-of-interest were selected away from tissue interfaces.

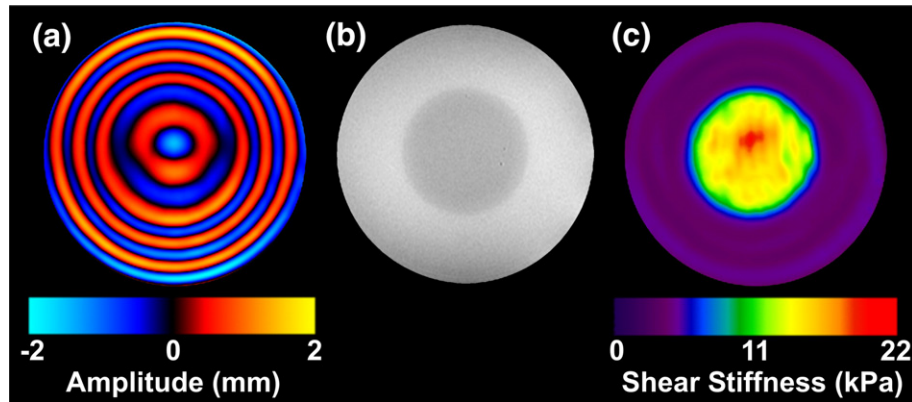


Fig. 3. (a) Image depicting shear waves propagating in the tissue-simulating gel phantom. Shear waves at 100 Hz were applied to the gel cylinder using the actuator in Fig. 2a. This image is one of eight that were acquired, each providing a quantitative depiction of the deformation of the medium caused by the propagating waves at a different time point in the wave cycle. The circular cross section of the stiff inclusion can be identified in the image because the wavelength of the propagating shear waves is longer in the stiffer material. (b) A GRE image indicates the location of the stiff inclusion. (c) The elastogram obtained from the wave data in (a) using the spatiotemporal directional filters and the LFE algorithm.

Tissue-simulating phantom

A tissue-simulating phantom was created to demonstrate the brain MRE imaging and reconstruction protocol using a very basic model of the vibration of the head. The geometry was chosen to provide a simple axial skull model with waves propagating from the edge to the center. The gelatin concentrations were chosen to approximate the shear stiffness values of brain tissue. The phantom consisted of a 9.5-cm diameter cylinder of 19% bovine gelatin surrounded by 10% bovine gelatin within a 20-cm diameter rigid cylinder. Axial imaging planes were acquired and 1-L reference phantoms were made from the same batches of gel used to con-

struct the phantom for separate testing to verify the inversion results. All phantoms were scanned at a mechanical excitation frequency of 100 Hz. This was done to match the frequency used in the human study.

Human studies

Cerebral elastography studies were performed in 25 healthy adult volunteers. All MRE examinations were performed with IRB approval and informed consent. The volunteers ranged in age from 23 to 79 years, with a mean age of 42.4 years. An operating frequency of 100 Hz was chosen as a compromise between wave

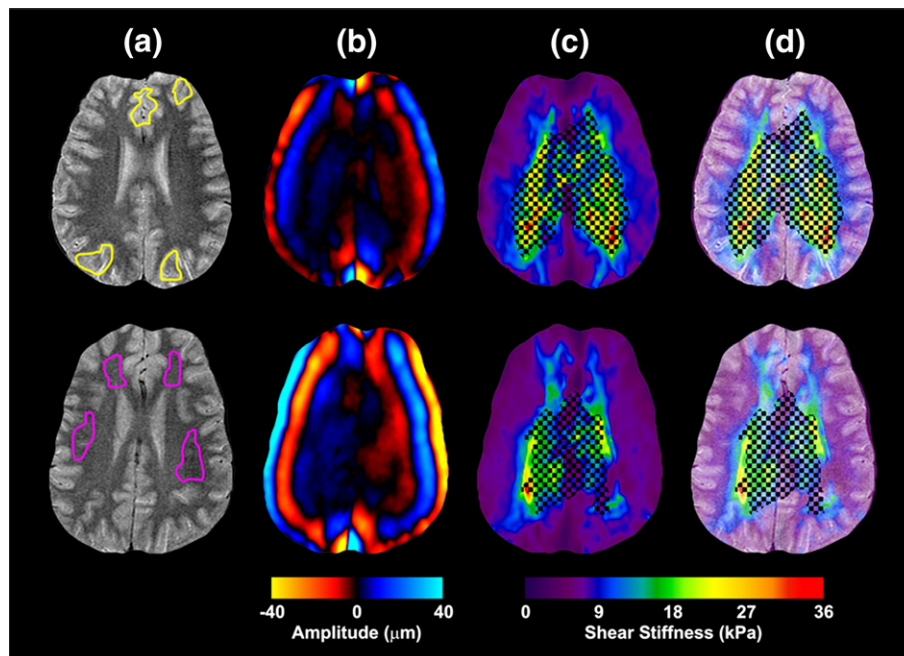


Fig. 4. Results from the MRE experiment performed on 2 different volunteers aged 25 and 23 using 100-Hz mechanical excitations. (a) T2-weighted FSE images for anatomical reference. The ROIs for gray matter and white matter are indicated in the top and bottom rows respectively. (b) Images indicating the shear waves propagating in the brain. The shear waves propagate from the perimeter of the brain inward. (c) The shear stiffness maps computed from the local frequency estimate (LFE) algorithm. A threshold, based on a phase difference SNR of 5:1, was applied to the shear stiffness estimates to mask regions with low displacement amplitude. (d) The shear stiffness maps overlaid on the anatomical reference illustrate the correlation of stiffness changes to anatomy.

penetration depth and the spatial resolution of the inversion algorithms. This level of vibration falls well below the conservative European Union whole body vibration standard (Ehman et al., 2007) designed to limit chronic occupational vibration exposure. Our IRB approved this guideline as one that would pose non-significant risk to our volunteers. MRE phase difference images were acquired after obtaining T2-weighted images to ensure proper slice selection and to provide an anatomical comparison map.

Results

Tissue-simulating phantom

MR elastographic imaging of the gelatin phantom at an actuator frequency of 100 Hz demonstrated a systematic change in the wavelength reflecting the underlying shear stiffness difference between the center and the surrounding gelatin of the phantom (Fig. 3). The mean shear stiffness for the inclusion was 13.5 ± 0.6 kPa and the shear stiffness of the reference gel was 14.2 ± 0.1 kPa. The background gel had a lower shear stiffness of 3.38 ± 0.07 kPa; the corresponding reference gel was 3.28 ± 0.06 kPa.

Human studies

Studying the data from the *in vivo* human studies, shear waves originated from the surface of the brain at the dural attachments and the falx (Fig. 4b). The wave fronts approach the gray/white matter junction in a parallel fashion. The figure also shows that as the waves propagate toward the center of the brain, the waves rapidly attenuate. The wavelength of the traveling shear wave increases as it proceeds inward, which indicates that it is traveling through increasingly stiffer media.

Quantitative shear stiffness maps were computed from the wave image data sets. Fig. 4 shows two typical shear stiffness maps (from two different volunteers) with their corresponding T2-weighted images. Due to attenuation, the SNR in the central regions is too

low for accurate inversions (as indicated by the crosshatch pattern in the elastograms). However, the SNR is suitable in the gray matter and partway into the white matter, and an increase in shear stiffness is clearly seen at the transition from gray matter to white matter.

Fig. 5 shows shear stiffness measurements obtained from the volunteers ($n=25$). The mean shear stiffness of cerebral white matter was 13.6 kPa (95% CI 12.3 to 14.8 kPa), while the elasticity of gray matter was lower at 5.22 kPa (95% CI 4.76 to 5.66 kPa). The difference was statistically significant ($p < 0.0001$). No apparent age trend was observed in the stiffness of the gray or white matter.

Discussion

This study shows that quantitative measurements of the shear stiffness of intracranial tissues are feasible with MRE. The results indicate that cerebral white matter is significantly stiffer than gray matter *in vivo*. Even with the limitations and assumptions of the LFE algorithm the values of the shear stiffness appear to correlate well with the visualized anatomy of the brain (Fig. 4). To date there is no definitive method for confirming estimates of brain stiffness *in vivo*. In fact, most estimates of brain elasticity in the literature (Fig. 1) were obtained *ex vivo*, from specimens without blood pressure and metabolic activity. This may explain why these estimates span an order of magnitude, and why there is not even consensus on whether gray matter is softer or stiffer than white matter (e.g., Nagashima et al., 1990, assumed gray matter to be stiffer than white matter for a finite element simulation of brain edema and Green et al. (2006), found gray matter to be stiffer than white matter with MRE). While no age-dependent trend in brain tissue stiffness was observed in this study, the current cohort of volunteers was not large enough to statistically determine age-dependent changes in the gray matter and white matter stiffness. If there are very small changes in stiffness with age, the sensitivity of our current technique may not allow for that assessment.

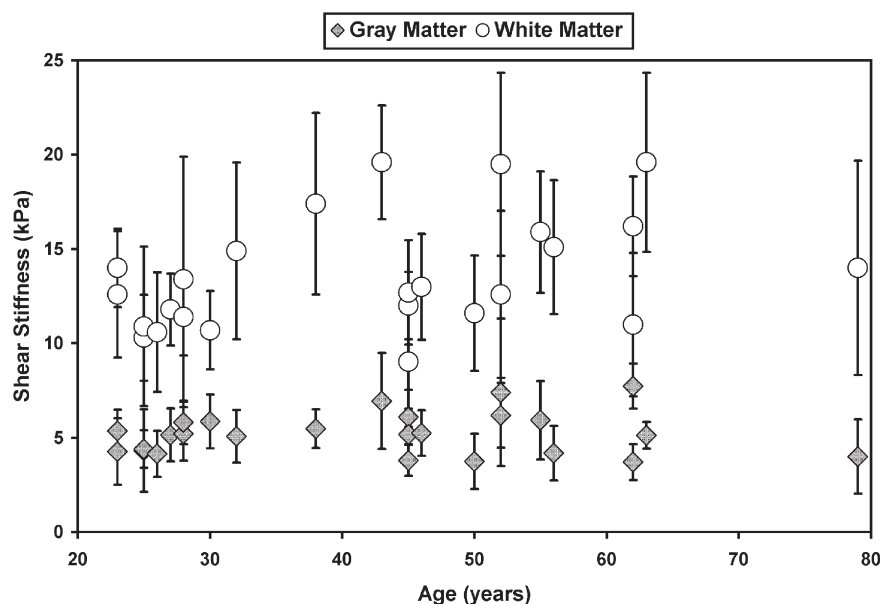


Fig. 5. Shear stiffness measurements for the age study volunteers obtained at 100 Hz.

This dynamic MRE technique has advantages over other previously described imaging techniques for measuring tissue stiffness *in vivo*. For example, static and quasi-static MRE (Plewes et al., 2000) techniques require compression of the tissue through hundreds of microns for tens or hundreds of milliseconds, which is not practical to do non-invasively. Ultrasound elasticity (Cespedes et al., 1993; Ophir et al., 1991) imaging of the *in vivo* brain would be extremely difficult due to the lack of an acoustic window through the skull.

Developments in the acquisition and reconstruction of MRE data may provide a better understanding of the underlying mechanical properties of tissue. Multi-slice, multi-echo techniques like fast spin-echo (FSE) (Grimm et al., 2001; Rydberg et al., 2001) and echo planar imaging (EPI) (Braun et al., 2002) sequences can image a larger volume of the brain in the same amount of time as the current GRE implementation. Impulse displacements and transient MRE can also be used to determine the mechanical properties of the brain by tracking a single wave front across the entire brain (McCracken et al., 2003, 2001).

Two-dimensional (2D) images were obtained in this study so that acquisition times could be limited to 3 min. It has been shown that 2D MRE is a good approximation of the three-dimensional (3D) wave propagation in the brain (Kruse and Ehman, 2003). However, true 3D imaging would better account for the geometrically complex nature of the wave propagation, including boundary effects and guided wave propagation. This approach would also allow for studies of the possible anisotropic properties of white matter tracts. Green et al. and Hamhaber et al. used 3D inversions for the data reported in Fig. 1 (Green et al., 2006, 2005; Hamhaber et al., 2007). This may explain the lower shear stiffness values for gray matter, white matter and average brain tissue. MRE data could also be obtained at several shear wave frequencies for each volunteer. From such data, frequency-dependent *viscous* properties of cerebral tissue can be studied (Kruse et al., 2000). These results show promise for the *in vivo* assessment of the mechanical properties of cerebral tissue and merit further exploration. It currently is not known exactly how much, if at all, the stiffness of brain tissue changes during certain disease processes (e.g., Alzheimer's disease). Therefore, it is too early to claim limits in the detection ability of MRE. Further improvements in the data acquisition and processing techniques will improve the precision of brain MRE and may allow for improved distinction between normal and pathologic tissue.

References

- Arbogast, K.B., Margulies, S.S., 1998. Material characterization of the brainstem from oscillatory shear tests. *J. Biomech.* 31 (9), 801–807.
- Auld, B.A., 1990. *Acoustic Fields and Waves in Solids*. Krieger Publishing Company, 21–38 pp.
- Bilston, L.E., Liu, Z.Z., Nhan, P.T., 1997. Linear viscoelastic properties of bovine brain tissue in shear. *Biorheology* 34 (6), 377–385.
- Bishop, J., Poole, G., Leitch, M., Plewes, D.B., 1998. Magnetic resonance imaging of shear wave propagation in excised tissue. *J. Magn. Reson. Imaging* 8 (6), 1257–1265.
- Bradley, W.G., Whittemore, A.R., Watanabe, A.S., Davis, S.J., Teresi, L.M., Homyak, M., 1991. Association of deep white matter infarction with chronic communicating hydrocephalus: implications regarding the possible origin of normal pressure hydrocephalus. *AJNR Am. J. Neuroradiol.* 12, 31–39.
- Braun, J., Bernarding, J., Tolxdorff, T., Sack, I., 2002. *In Vivo Magnetic Resonance Elastography of the Human Brain Using Ultrafast Acquisition Techniques*. International Society for Magnetic Resonance in Medicine, Honolulu, Hawaii, USA, p. 2597. May 18–24.
- Burlew, M.M., Madsen, E.L., Zagzebski, J.A., Banjavic, R.A., Sum, S.W., 1980. A new ultrasound tissue-equivalent material. *Radiology* 134 (2), 517–520.
- Cespedes, I., Ophir, J., Ponnekanti, H., Maklad, N., 1993. Elastography: elasticity imaging using ultrasound with application to muscle and breast *in vivo*. *Ultrason. Imag.* 15, 73–88.
- Chenevert, T.L., Skovoroda, A.R., O'Donnell, M., Emelianov, S.Y., 1998. Elasticity reconstructive imaging by means of stimulated echo MRI. *Magn. Reson. Med.* 39 (3), 482–490.
- Donnelly, B.R., Medige, J., 1997. Shear properties of human brain tissue. *J. Biomech. Eng.* 119 (4), 423–432.
- Duck, F.A., 1990. *Physical Properties of Tissue—A Comprehensive Reference Book*. Academic Press, San Diego, CA. 225–248 pp.
- Ehman, E., Rossman, P., Kruse, S., 2007. Vibration Safety Limits for Magnetic Resonance Elastography. International Society for Magnetic Resonance in Medicine, Berlin, Germany, p. 1257. May 19–25.
- Ehman, R.L., Muthupillai, R., Lomas, D.J., Rossman, P.J., Greenleaf, J.F., Manduca, A., 1995. Magnetoelastography—MR-imaging of acoustic strain waves. *Radiology* 197, 355.
- Estes, M.S., McElhaney, J.H., 1970. Response of brain tissue of compressive loading. American Society of Mechanical Engineers: Paper No. 70-BHF-13.
- Fallenstein, G.T., Hulce, V.D., Melvin, J.W., 1969. Dynamic mechanical properties of human brain tissue. *J. Biomech.* 2, 217–226.
- Felmlee, J.P., Rossman, P.J., Muthupillai, R., Manduca, A., Dutt, V., Ehman, R.L., 1997. Magnetic Resonance Elastography of the Brain: Preliminary In Vivo Results. International Society for Magnetic Resonance in Medicine, Vancouver, B.C., Canada, p. 683. April 12–18.
- Fowlkes, J.B., Emelianov, S.Y., Pipe, J.G., Skovoroda, A.R., Carson, P.L., Adler, R.S., Sarvazyan, A.P., 1995. Magnetic resonance imaging techniques for detection of elasticity variation. *Med. Phys.* 22 (11 Pt 1), 1771–1778.
- Galford, J.E., McElhaney, J.H., 1970. A viscoelastic study of scalp, brain, and dura. *J. Biomech.* 3 (2), 211–221.
- Graff, K.F., 1991. *Wave Motion in Elastic Solids*. Dover, New York. 278–281 pp.
- Green, M., Sinkus, R., Bilston, L.E., 2006. High Resolution 3D Brain MR-Elastography. International Society for Magnetic Resonance in Medicine, Seattle, Washington, USA, p. 2021. May 6–12.
- Green, M., Sinkus, R., Cheng, S., Bilston, L., 2005. 3D MR-Elastography of the Brain at 3tesla. International Society for Magnetic Resonance in Medicine, Honolulu, Hawaii, USA, p. 2176. May 7–13.
- Grimm, R., Rydberg, J., Ehman, R., 2001. Phase Difference Encoding of Coherent Pathways for High Speed MR Elastography. International Society for Magnetic Resonance in Medicine, Glasgow, Scotland, p. 1636. April 21–27.
- Hamhaber, U., Sack, I., Papazoglou, S., Rump, J., Braun, J., 2007. Three-dimensional analysis of shear wave propagation observed by *in vivo* magnetic resonance elastography of the brain. *Acta Biomater.* 3, 127–137.
- Hirakawa, K., Hashizume, K., Hayashi, T., 1981. Viscoelastic property of human brain—for the analysis of impact injury (author's translation). *No To Shinkei* 33 (10), 1057–1065.
- Kleiven, S., Hardy, W.N., 2002. Correlation of an FE model of the human head with local brain motion—consequences for injury prediction. *Stapp Car Crash J.* 46, 123–144.
- Knutsson, H., Westin, C.-F., Granlund, G., 1994. Local Multiscale Frequency and Bandwidth Estimation. IEEE Computer Society, Los Alamitos, CA, pp. 36–40.
- Kruse, S.A., Dresner, M.A., Rossman, P., Felmlee, J.P., Jack, C.R., Ehman, R.L., 1999. Palpation of the Brain Using Magnetic Resonance Elastography. International Society for Magnetic Resonance in Medicine, Philadelphia, Pennsylvania, USA, p. 258. May 22–28.
- Kruse, S.A., Ehman, R.L., 2003. 2D Approximation of 3D Wave Propagation in MR Elastography of the Brain. International Society for

- Magnetic Resonance in Medicine, Toronto, Ontario, Canada, p. 1084. July 10–16.
- Kruse, S.A., Smith, J.A., Lawrence, A.J., Dresner, M.A., Manduca, A., Greenleaf, J.F., Ehman, R.L., 2000. Tissue characterization using magnetic resonance elastography: preliminary results. *Phys. Med. Biol.* 45, 1579–1590.
- Lewa, C.J., de Certaines, J.D., 1995. MR imaging of viscoelastic properties. *J. Magn. Reson. Imaging* 5 (2), 242–244.
- Ljung, C., 1975. A model for brain deformation due to rotation of the skull. *J. Biomech.* 8 (5), 263–274.
- Manduca, A., Lake, D.S., Kruse, S.A., Ehman, R.L., 2003. Spatio-temporal directional filtering for improved inversion of MR elastography images. *Med. Image Anal.* 7, 465–473.
- Manduca, A., Muthupillai, R., Rossman, P.J., Greenleaf, J.F., Ehman, R.L., 1996. Image processing for magnetic resonance elastography. In: Loew, M.H., Hanson, K.M. (Eds.), *SPIE Proceedings Series. SPIE—The International Society for Optical Engineering*, Newport Beach, California, USA, pp. 616–623.
- Manduca, A., Oliphant, T.E., Dresner, M.A., Mahowald, J.L., Kruse, S.A., Amromin, E., Felmlee, J.P., Greenleaf, J.F., Ehman, R.L., 2001. Magnetic resonance elastography: non-invasive mapping of tissue elasticity. *Med. Image Anal.* 5, 237–254.
- McCracken, P.J., Manduca, A., Ehman, R.L., 2003. MR Elastography for Studying the Biomechanics of Traumatic Brain Injury. *International Society for Magnetic Resonance in Medicine*, Toronto, Ontario, Canada, p. 799. July 10–16.
- McCracken, P.J., Manduca, A., Felmlee, J.P., Ehman, R.L., 2001. Mechanical transient-based method for MR elastography. *Radiology* 221P, 329.
- Metz, H., McElhane, J., Ommaya, A.K., 1970. A comparison of the elasticity of live, dead, and fixed brain tissue. *J. Biomech.* 3 (4), 453–458.
- Miga, M.I., Paulsen, K.D., 2000. In vivo quantification of a homogeneous brain deformation model for updating preoperative images during surgery. *IEEE Trans. Biomed. Eng.* 47 (2), 266–273.
- Miller, K., 1999. Constitutive model of brain tissue suitable for finite analysis of surgical procedures. *J. Biomech.* 32, 531–537.
- Moore, D., Pursley, R., Dimitriadis, E., Talagala, S., 2003. Magnetic Resonance Imaging of Brain Transverse Acoustic Waves. *International Society for Magnetic Resonance in Medicine*, Toronto, Ontario, Canada, p. 2298. July 10–16.
- Muthupillai, R., Ehman, R.L., 1996. Magnetic resonance elastography. *Nat. Med.* 2 (5), 601–603.
- Muthupillai, R., Lomas, D.J., Rossman, P.J., Greenleaf, J.F., Manduca, A., Ehman, R.L., 1995. Magnetic resonance elastography by direct visualization of propagating acoustic strain waves. *Science* 269 (5232), 1854–1857.
- Muthupillai, R., Rossman, P.J., Lomas, D.J., Greenleaf, J.F., Riederer, S.J., Ehman, R.L., 1996. Magnetic resonance imaging of transverse acoustic strain waves. *Magn. Reson. Med.* 36 (2), 266–274.
- Nagashima, T., Shirakuni, T., Rapoport, S.I., 1990. A two-dimensional, finite element analysis of vasogenic brain edema. *Neurol. Med.-Chir. (Tokyo)* 30 (1), 1–9.
- Oliphant, T.E., Manduca, A., Ehman, R.L., Greenleaf, J.F., 2001. Complex-valued stiffness reconstruction for magnetic resonance elastography by algebraic inversion of the differential equation. *Magn. Reson. Med.* 45, 99–310.
- Ophir, J., Cespedes, I., Ponnekanti, H., Yazdi, Y., Li, X., 1991. Elastography: a quantitative method for imaging the elasticity of biological tissues. *Ultrason. Imag.* 13 (2), 111–134.
- Parker, K.J., Huang, S.R., Musulin, R.A., Lerner, R.M., 1990. Tissue response to mechanical vibrations for “sonoelasticity imaging”. *Ultrasound Med. Biol.* 16 (3), 241–246.
- Parker, K.J., Lerner, R.M., 1992. Sonoelasticity of organs: shear waves ring a bell. *J. Ultrasound Med.* 11 (8), 387–392.
- Plewes, D.B., Betty, I., Urchuk, S.N., Soutar, I., 1995. Visualizing tissue compliance with MR imaging. *J. Magn. Reson. Imaging* 5 (6), 733–738.
- Plewes, D.B., Bishop, J., Samani, A., Sciarretta, J., 2000. Visualization and quantification of breast cancer biomechanical properties with magnetic resonance elastography. *Phys. Med. Biol.* 45, 1591–1610.
- Roberts, D.W., Miga, M.I., Hartov, A., Eisner, S., Lemery, J.M., Kennedy, F.E., Paulsen, K.D., 1999. Intraoperatively updated neuroimaging using brain modeling and sparse data. *Neurosurgery* 45 (5), 1199–1206.
- Rose, G.H., Dresner, M.A., Rossman, P.J., Felmlee, J.P., Muthupillai, R., Ehman, R.L., 1998. Palpation of the brain using magnetic resonance elastography. *Radiology* 209P, 1268.
- Rydberg, J., Grimm, R., Kruse, S., Felmlee, J., McCracken, P., Ehman, R., 2001. Fast Spin-Echo Magnetic Resonance Elastography of the Brain. *International Society for Magnetic Resonance in Medicine*, Glasgow, Scotland, p. 1647. April 21–27.
- Sarvazyan, A., Goukassian, D., Maevisky, E., Skovoroda, A., Emelianov, S., 1994. Elasticity Imaging as a New Modality of Medical Imaging for Cancer Detection. In: *Proceedings of International Workshop on Interaction of Ultrasound with Biological Media*, pp. 69–81. 5–9 April. Valenciennes, France.
- Shuck, L.Z., Advani, S.H., 1972. Rheological response of human brain tissue in shear. *J. Basic Eng.* 94, 905–911.
- Smith, J.A., Muthupillai, R., Rossman, P.J., Hulshizer, T.C., Greenleaf, J.F., Ehman, R.L., 1997. Characterization of biomaterials using magnetic resonance elastography. In: Thompson, D.O., Chimenti, D.E. (Eds.), *Review of Progress in Quantitative Nondestructive Evaluation*. Plenum Press, New York, pp. 1323–1330.
- Uffmann, K., Maderwald, S., de Greiff, A., Ladd, M.E., 2004. Determination of Gray and White Matter Elasticity with MR Elastography. *International Society for Magnetic Resonance in Medicine*, Kyoto, Japan, p. 1768. May 15–21.
- Van Houten, E.E.W., Miga, M.I., Weaver, J.B., Kennedy, F.E., Paulsen, K.D., 1999. An overlapping subzone technique for MR-based elastic property reconstruction. *Magn. Reson. Med.* 42, 779–786.
- Walsh, E.K., Schettini, A., 1976. Elastic behavior of brain tissue in vivo. *Am. J. Physiol.* 230 (4), 1058–1062.
- Wang, H.C., Wineman, A.S., 1972. A mathematical model for the determination of viscoelastic behavior of brain in vivo. I. Oscillatory response. *J. Biomech.* 5 (5), 431–446.
- Xu, L., Lin, Y., Xi, Z.N., Shen, H., Gao, P.Y., 2007. Magnetic resonance elastography of the human brain: a preliminary study. *Acta Radiol.* 48 (1), 112–115.
- Zhang, L., Yang, K.H., Dwarampudi, R., Omori, K., Li, T., Chang, K., Hardy, W.N., Khalil, T.B., King, A.I., 2001. Recent advances in brain injury research: a new human head model development and validation. *Stapp Car Crash J.* 45, 369–394.